Isotropic Holographic Metasurfaces for Dual-Functional Radiations without Mutual Interferences

*Yun Bo Li, Ben Geng Cai, Qiang Cheng, and Tie Jun Cui**

The dual-functional and/or multifunctional devices have huge fascinations and prospects to conveniently integrate complex systems with low costs. However, most of such devices are based on anisotropic media or anisotropic structures. Here, a new method is proposed to design planar dual-functional devices using an isotropic holographic metasurface, in which two different functions are written on the same holographic interference pattern with no mutual coupling. When the metasurface is excited by two orthogonally ported sources, the corresponding dual functions can be controlled by the object waves, which are not affected by each other due to suppression of mutual interference. The proposed metasurface is composed of subwavelength-scale isotropic metallic patches on a grounded dielectric. In this specific design, double-beam and double-polarization radiate devices are realized independently by the orthogonal excitations. Based on the theoretical analysis, scanning radiate beams that are only controlled by frequency with different performances under orthogonal polarizations are demonstrated. To the best of our knowledge, this is the first time for actualizing dual-functional devices using isotropic textures. Full-wave simulations and experimental results in the microwave frequencies are presented to validate the proposed theory and confirm the corresponding physical phenomena.

1. Introduction

Due to the extreme abilities to control electromagnetic (EM) waves, metasurfaces have been overwhelmingly investigated in recent years. Compared to the previous bulk metamaterials,[1–3] metasurfaces have many advantages such as low loss, low cost, and high performance. There are two existing methods in modeling metasurfaces. One is called as the generalized sheet transition conditions,[4,5] which can be used to modulate spatial waves; and the other is the transverse resonance approach,[6] which can be applied to control surface waves. Such two methods can mathematically explain almost all phenomena in metasurfaces. Combining with classical EM theories such as the Babinet principle, Snell's law, and Huygens principle, the milepost-type works on metasurfaces have been proposed.[7–9] Consequently, many outstanding phenomena in controlling the microwave and optical wavefronts have been reported.[10–19]

Holographic metasurfaces, which can generate arbitrary optical images and wavefronts under different designs of interference patterns, have played important roles in the field of metasurface. By using complementary V-type nano-antennas, Ni et al. proposed the thinnest hologram to modulate both amplitudes and phases in the optical band, which can generate high-resolution and low-noise images.[20] Meanwhile, Zhang's group used the plasmonic metasurfaces to reconstruct the image of complex object in visual band by eliminating the undesired effects of multiple diffractions.[21] Then the same group made metaholograms to reach 80% conversion efficiency between two circular-polarization states,[22] hence it is hopeful to apply metasurface holograms in fabricating optical devices. In the infrared band, metamaterial phase holograms have also been presented.[23]

In the infrared and optical frequencies, the reproduction of object images is the key problem in the holographic[24] or calculation holographic[25] technology. However, in the microwave frequencies and radar systems, holographic radiations are the most important topics. The theory of holographic antenna is similar to that of holographic image, in which the radiate wave is defined as the object wave. By using the quasi-periodic metasurface, a method to shape surface waves excited by monopole source to circularly polarized radiate waves has been introduced.[26] Combining with the leaky-wave theory, Patel and Grbic designed a 1D printed leaky-wave holographic antenna and proposed a fast algorithm to extract the surface impedance of metasurface texture to replace the eigen-mode simulations.[27] Later, a special holographic metasurface was presented to generate multiple radiate beams and make the beams scanning with frequency in the 2D manner.[28]

Recently, some important advances have been achieved to produce dual-functional devices using metamaterials, including an optical "Janus" device made of bulk metamaterial for

Y. B. Li, B. G. Cai, Prof. Q. Cheng, Prof. T. J. Cui
State Key Laboratory of Millimeter Waves
Southeast University
Nanjing 210096, P. R. China
E-mail: tjcui@seu.edu.cn
Prof. Q. Cheng, Prof. T. J. Cui
Cooperative Innovation Centre of Terahertz Science
No. 4, Section 2
North Jianshe Road, Chengdu 610054, P. R. China

DOI: 10.1002/adfm.201503654

focusing lens and beam shifter,[29] and a bifunctional planar Luneburg-fisheye lens made of metasurface to control surface waves.[30] Most importantly, the dual-functional holographic images in the visible band have been reported.[31–33] However, these dual-functional devices were based on anisotropic unit cells, which are difficult to design and realize.[29–33] To the best of our knowledge, dual-functional holographic metasurfaces made of isotropic structures have not been reported to control the beam radiations independently.

Here, we propose a general method to design and realize dual-functional holographic radiate devices using *isotropic* metasurfaces without mutual interference. Compared to the literatures relevant to the single-functional holographic antennas,[26–28] we accomplish the dual-functional design in a single conjunct aperture. Compared to the former dual-functional devices, the proposed holographic metasurface is only composed of isotropic textures, which has less complexity for the unit-cell design and can eliminate the mutual interference between such two functions. Based on the holographic theory, we simultaneously record two arbitrary functions (object waves) on a single holographic pattern generated by interference with two orthogonally ported monopole sources (reference waves). We find that each function can be realized by exciting the corresponding reference wave, and the result of function reproduction is nearly irrelevant to the other function. Based on the good performance in suppressing the mutual calculation hologram, we design two dual-functional devices, one of which realizes double-beam radiations under the same polarization, while the other of which realizes single-beam radiations with orthogonal polarizations. Based on our theoretical analysis, for the horizontal polarization, the radiate beam can complete 1D (along the elevation direction) spatial scanning. However, for the vertical polarization, the radiate beam can accomplish 2D (along both elevation and azimuth directions) spatial scanning. The excellent performance of dual-functional radiate devices promises huge potentials of metasurface in developing new imaging systems and radar systems.

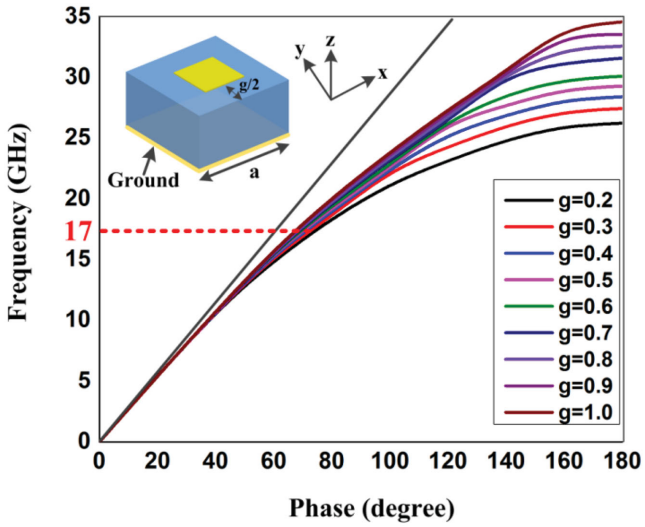

Figure 1. The dispersion curves of the metasurface unit cells (inset) with different gaps, in which the black oblique line indicates the light line in free space. Here, the lattice's period is $a = 3$ mm; a commercially printed circuit board F4B is chosen as the dielectric substrate with the relative permittivity $\varepsilon_r = 2.2$; and the thickness $t = 1.57$ mm.

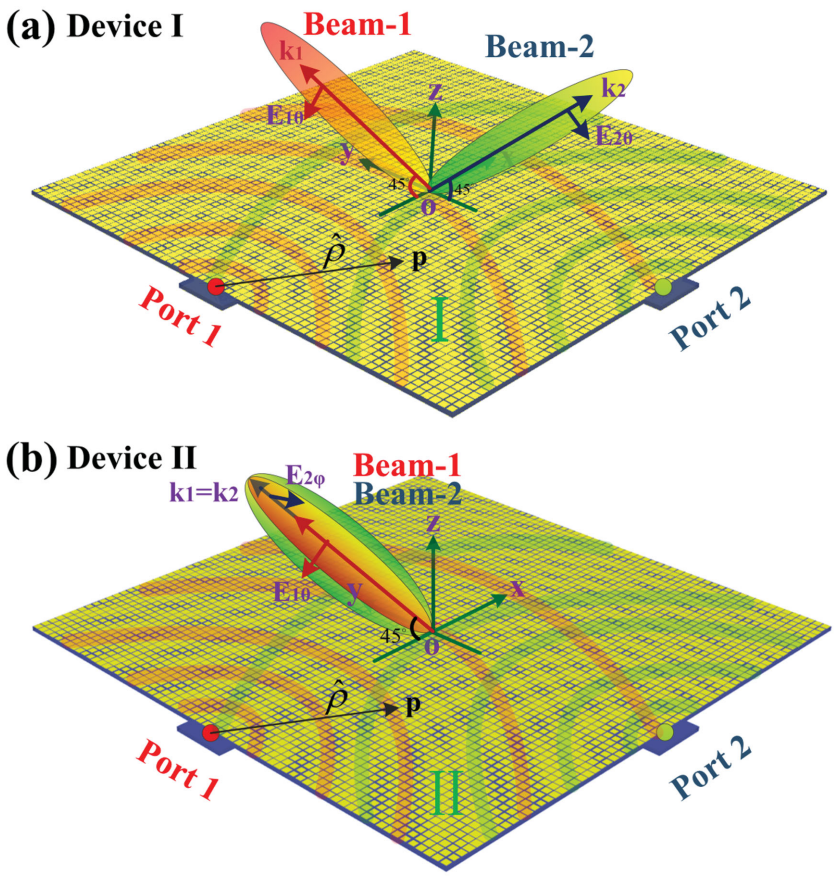

Figure 2. Schematics of two dual-functional holographic metasurface devices. a) Device I: Double-beam radiations with the same polarization state. b) Device II: Single-beam radiations with orthonormal polarizations.

2. Design of the Dual-Functional Devices

2.1. Concept of the Dual-Functional Devices

According to the calculation holographic theory,[25] we can get the desired object wave by exciting the hologram which is interfered by the object and reference waves. The hologram is generally defined as $\Psi = |\psi_{ref} + \psi_{obj}|$, in which ψ_{ref} and ψ_{obj} represent the reference wave and object wave, respectively. Based on the surface impedance technology, the hologram can be shaped by subwavelength-scale quasi-periodic surface-impedance textures,[34,35] and the distributions of surface impedance are given by

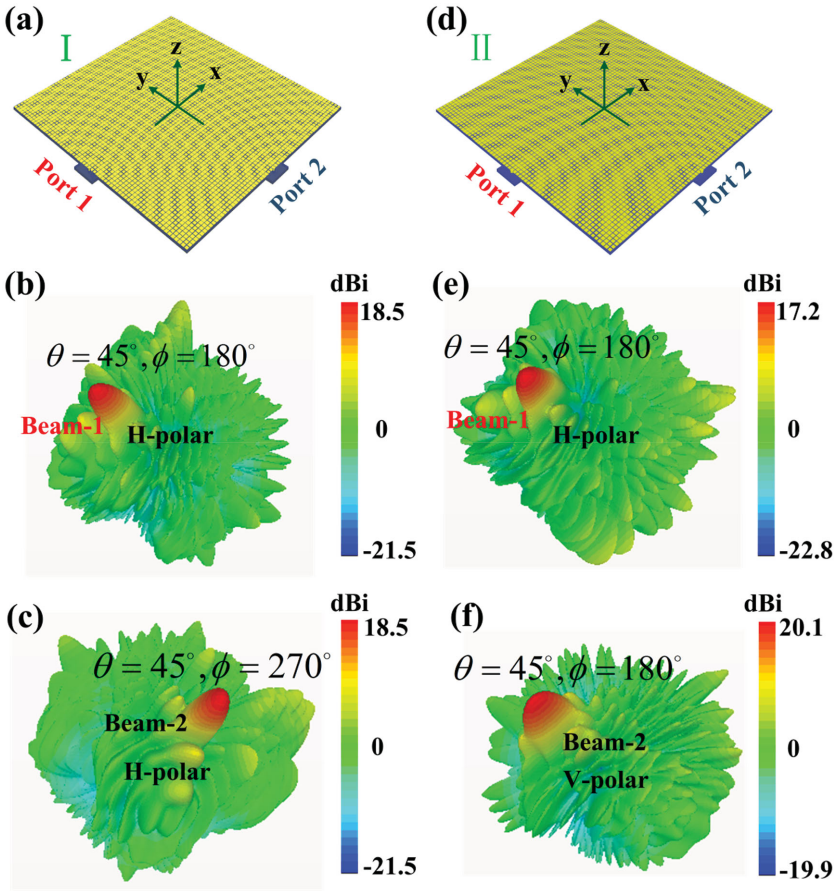

Figure 3. Full-wave simulation results of the two dual-functional holographic metasurface devices. a–c) Device (I) for copolarized two-beam radiations under different excitations. d–f) Device (II) for cross-polarized single-beam radiations under different excitations.

$$Z = j\,[X + M\mathrm{Re}(\psi_{\mathrm{ref}}^{*}\psi_{\mathrm{obj}})] \tag{1}$$

where X and M indicate the average surface impedance and the modulation depth, respectively, and "*" represents the complex conjugation. If the surface-impedance hologram recorded as Equation (1) is excited by the reference wave, the object wave which is considered as the realization function can be reproduced. To realize dual-functional devices, we define a general distribution of surface impedance as

$$Z = j\left[X + \frac{1}{2}M\mathrm{Re}(\psi_{\mathrm{ref1}}^{*}\psi_{\mathrm{obj1}}) + \frac{1}{2}M\mathrm{Re}(\psi_{\mathrm{ref2}}^{*}\psi_{\mathrm{obj2}})\right] \tag{2}$$

Hence the whole impedance hologram is the addition of two subholograms. In a specific design, we propose two dual-functional devices producing: (I) double-beam radiations with the same polarization and (II) single-beam radiations with orthonormal polarizations. In term of the function (I), we define

$$\begin{aligned}\psi_{\mathrm{ref1}} &= \exp(-jkn\sqrt{(x-x_0)^2+y^2}),\ \psi_{\mathrm{ref2}} = \exp(-jkn\sqrt{x^2+(y-y_0)^2}),\\ \psi_{\mathrm{obj1}} &= \exp(jkx\sin(45°)),\ \psi_{\mathrm{obj2}} = \exp(jky\sin(45°)),\end{aligned} \tag{3}$$

where k is the wavenumber in free space and n is the average surface refractive index of the holographic metasurface. The reference waves (ψ_{ref1} and ψ_{ref2}) are two surface cylindrical waves radiated from points $(x_0, 0)$ and $(0, y_0)$ on the metasurface; while the object waves (ψ_{obj1} and ψ_{obj2}) indicate two radiation waves directing to 45° angles with respect to the x and y axes, respectively. In term of function (II), to realize the single-beam radiation with orthonormal polarizations, we define

$$\psi_{\mathrm{obj1}} = \psi_{\mathrm{obj2}} = \exp(jkx\sin(45°)) \tag{4}$$

in which the reference waves are the same as those in (I). In fact, we can design arbitrary radiations of two beams by defining different reference and object waves.

2.2. Material Synthesis and Analysis of the Functionality

To describe the distribution of surface impedance, we choose the subwavelength-scale isotropic metallic patch as the basic unit cell, which is printed on a grounded substrate, as shown in **Figure 1** (inset). We use the eigen-mode simulation method in commercial software, CST Microwave Studio, to obtain the dispersion curves by changing the gap between two adjacent metallic patches. Because transverse-magnetic surface waves are supported by such unit cell, combining with the wavenumber equation, we derive the relationship between the phase difference ϕ across the unit cell (with period a) and the surface impedance as

$$Z_s = Z_0\sqrt{1-\phi^2c^2/a^2\omega^2} \tag{5}$$

in which c and Z_0 are the light speed and wave impedance in free space, while ω is the angular frequency. Then we apply cubic polynomials fitting to establish the relation between surface impedance Z_s and the gap size g, as illustrated in Figure 1.

According to Equations (2)–(4), we can utilize the metasurface unit cells to shape two impedance holograms for two dual-functional devices, as shown in **Figure 2**. To obtain different reproduction waves, we use the sources placed at "Port 1" and "Port 2" to excite the whole hologram. For the device function (I), the reproduced wave generated by excitation of "Port 1" is written as

$$\begin{aligned}\psi_{\mathrm{rep1}} &= \psi_{\mathrm{ref1}}(\psi_{\mathrm{ref1}}^{*}\psi_{\mathrm{obj1}}) + \psi_{\mathrm{ref1}}(\psi_{\mathrm{ref2}}^{*}\psi_{\mathrm{obj2}})\\ &= |\psi_{\mathrm{ref1}}|^2\psi_{\mathrm{obj1}} + \psi_{\mathrm{disturb}}\\ &= A\exp(jkx\sin(45°))\\ &\quad + \exp(-jkn\sqrt{(x-x_0)^2+y^2} + jkn\sqrt{x^2+(y-y_0)^2} + jky\sin(45°))\end{aligned} \tag{6}$$

We find that the reproduced wave has two terms, which are the desired functional wave $|\psi_{\mathrm{ref1}}|^2\psi_{\mathrm{obj1}} = A\exp(-jkx\sin(45°))$ ($A = |\psi_{\mathrm{ref1}}|^2$) and a disturbing wave ψ_{disturb}, respectively. According to the surface phase distribution of the functional wave, the radiation wave can be described as "Beam 1" in Figure 2a. However, by observing the disturbing wave, the

surface phase distribution is dispersive. Since the near-field surface current and far-field radiation pattern are pairs of spatial Fourier transform, we expect that the radiation power caused by the disturbing wave is disordered, and is much lower than that of the desired functional wave. Hence the proposed holographic metasurface has no mutual interference, especially when the metasurface aperture is large. Based on rotational symmetry, the circumstance of excitation by "Port 2" is the same as that by "Port 1." Hence the metasurface device (I) can realize the dual-beam radiations under different excitation ports.

For the holographic metasurface device (II), by analyzing Equations (4) and (6), the reproduced waves from excitations of "Port 1" and "Port 2" have the same radiation direction (see Figure 2b) without mutual interference, which are given as

$$\psi_{\text{rep1}} = A\exp(jkx\sin(45°)) \tag{7a}$$

$$\psi_{\text{rep2}} = B\exp(jkx\sin(45°)) \tag{7b}$$

in which $A = |\psi_{\text{ref1}}|^2$ and $B = |\psi_{\text{ref2}}|^2$. The surface electric field excited by the monopole source has two polarizations along z- and ρ-directions (from Port 1 or Port 2 to a point on metasurface). For the definition of surface impedance $Z_s = E_\rho/H_\phi$, we only design the radiation waves under the x (horizontal) and y (vertical) polarizations, depending on only the ρ-direction.

With regard to Beam 1 generated by Port 1 in Figure 2b, the surface electric field is considered as the main contribution to the desired functional wave, which can be expressed as

$$\psi_{\text{rep1}} = \hat{\rho}\ \exp(jkx\sin(45°))\left(\hat{\rho} = \frac{1}{|\rho|}((x-x_0)\hat{x} + \hat{y})\right) \tag{8}$$

The object wave has only horizontal polarization (x component) because the y component of surface electric field is symmetrical to the x-axis that results in the cancellation of the desired radiation by calculating the whole surface current integration. Similarly, although the x component of surface reproduced wave is asymmetrical to the y-axis, the two sides of y-axis on the metasurface will support the radiation with the opposite phase in the desired radiation direction, which causes the cancellation of horizontal-polarization radiation wave in the far fields. Thus, Beam 2 in Figure 2b has only vertical polarization.

Thus the two holographic metasurface devices have different dual-functional characteristics for double-beam radiations with the same polarization (I) and for single-beam radiations with orthonormal polarizations (II). The corresponding full-wave simulation results are presented in **Figure 3**. Due to the rotational symmetry of device (I), we consider that Beams 1 and 2 have the same polarization (H-polar) state by rotating the coordinate system by 90°.

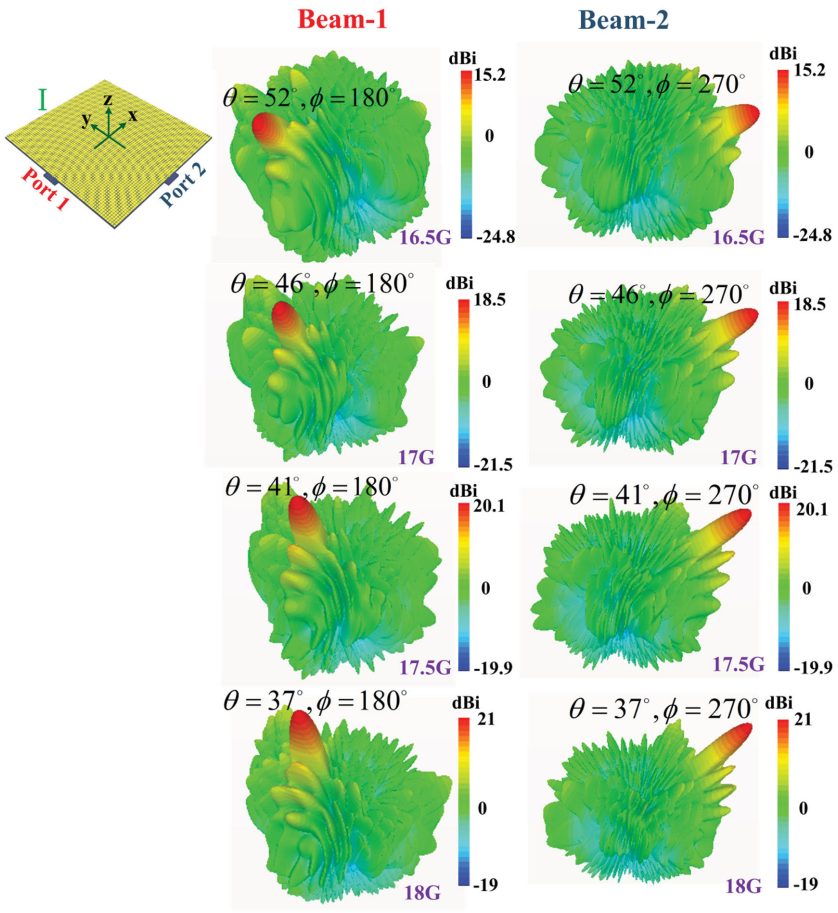

Figure 4. Full-wave simulation results of the holographic metasurface device (I). The two ports generate the dual-beam radiations with 1D frequency scanning from 16.5 to 18 GHz.

2.3. New Physical Phenomenon of the Two Dual-Functional Devices

The performance of the holographic radiations can be interpreted by the backward leaky-wave principle of the "–1"-order Floquet's mode. In general, we define the object wave as $\psi_{\text{obj}} = e^{jk\sin(\theta)[x\cos(\varphi)+y\sin(\varphi)]}$ and the reference wave as $\psi_{\text{ref}} = e^{-jkn\rho}$ (the same as ψ_{ref1} in Equation (3). Here, we remark that the sinusoidal phase distribution of hologram shaped by the impedance units is approximately invariant by changing the frequency because the higher- and lower-impedance areas of the hologram are fixed. If we use the incoherent reference wave $\psi'_{\text{ref}} = e^{-jk'n'\rho}$ (k' and n' are the wavenumber and effective surface refractive index under the incoherent frequency) to excite the impedance metasurface, according to Equation (1) and ignoring the mutual interference in terms of above analysis, the phase of the reproductive surface electric field is described as

$$\Phi = -k'n'\rho + kn\rho + k\sin(\theta)[x\cos(\varphi) + y\sin(\varphi)] \tag{9}$$

When the surface wavefront generated by Port 1 of device (I) propagates to point P (see Figure 2a) along the ρ-direction, the phase of surface wave along the x-direction is expressed as $\Phi_x = -(k'n' - kn)(x - x_0) + kx\sin(\theta)\cos(\varphi)$. Similarly, the phases along the y and $-y$-directions are expressed

as $\Phi_{+y} = -(k'n' - kn)y + ky\sin(\theta)\sin(\varphi)$ and $\Phi_{-y} = (k'n' - kn)y + ky\sin(\theta)\sin(\varphi)$. For device (I), $\theta = 45°$ and $\varphi = 0°$, thus $\Phi_x = -(k'n' - kn)(x - x_0) + kx\sqrt{2}/2$ and the corresponding x component of effective surface wavenumber is $k_{sx} = -k'n' + kn + k\sqrt{2}/2$. Similarly, $\Phi_{\pm y}$ is written as $\mp (k'n' - kn)y$, and the corresponding y component of surface wavenumbers are $k_{+sy} = -k'n' + kn$ and $k_{-sy} = k'n' - kn$. As a consequence, for the $+y$ and $-y$ components of the metasurface, the total surface wavenumbers are $k_{s(+y)} = \sqrt{k_{sx}^2 + k_{+sy}^2}$ and $k_{s(-y)} = \sqrt{k_{sx}^2 + k_{-sy}^2}$.

Based on the above analysis, we expect that there are two radiate beams generated by the y and $-y$ components of the metasurface, respectively. To the y component, from the leaky-wave theory, the angles of radiation waves (leaky waves) can be give as $\theta_{I(+y)} = \arcsin(k_{s(+y)}/k)$ and $\varphi_{I(+y)} = \pi + \arctan(k_{+sy}/k_{sx})$. Similarly, to the $-y$ component, the radiation angles are described by $\theta_{I(-y)} = \arcsin(k_{s(-y)}/k)$ and $\varphi_{I(-y)} = \pi + \arctan(k_{-sy}/k_{sx})$. Hence we expect that there are two radiation waves generated by the whole metasurface of device (I) under the excitation of Port 1, and the two radiation waves can be physically combined into a single beam under small changes of incoherent frequency in the far fields. It is obvious that the azimuth angle of the combination beam is π. When the incoherent frequency is varied significantly, the two radiate beams can be distinguished.

Because the surface reproduced wave is symmetrical to the x-axis, the component of the vertical polarization in the desired radiation direction does not exist. Thus the object wave generated by Port 1 in device (I) can complete the 1D frequency scanning under the horizontal polarization, and the corresponding simulation results are shown in **Figure 4**, in which the azimuth angle remains π. Due to the rotating symmetry, the same result will occur under the Port 2 excitation, as demonstrated in Figure 4.

For the holographic metasurface device (II), the characteristics of frequency scanning generated by Port 1 are quite similar to those in device (I). However, under the excitation of Port 2 which generates the reproduced wave asymmetrically to the y-axis, the corresponding components of the effective surface wave phases are given as $\Phi_{+x} = -(k'n' - kn)x + kx\sqrt{2}/2$, $\Phi_{-x} = (k'n' - kn)x + kx\sqrt{2}/2$, and $\Phi_y = -(k'n' - kn)(y - y_0)$. We expect that there are two radiation waves generated by the x and $-x$ components of the metasurface, respectively. The angles of two radiation waves are given as $\theta_{II(+x)} = \arcsin(k_{s(+x)}/k)$, $\varphi_{II(+x)} = \pi + \arctan(k_{sy}/k_{+sx})$ and $\theta_{II(-x)} = \arcsin(k_{s(-x)}/k)$, $\varphi_{II(-x)} = \pi + \arctan(k_{sy}/k_{-sx})$, where k_{+sx}, k_{-sx}, $k_{s(+x)}$, $k_{s(-x)}$, and k_{sy} have the analogous definitions as those in device (I). Again, the two radiation waves can be combined to one beam under small changes of incoherent frequency. For the asymmetric hologram of device (II), after analyzing the expressions of $\theta_{II(+x)}$, $\varphi_{II(+x)}$, $\theta_{II(-x)}$, and $\varphi_{II(-x)}$ controlled by frequency, we conclude that the combination beam can accomplish the 2D frequency scanning under the vertical polarization, both in elevation and azimuth directions, as clearly demonstrated in the full-wave simulation results in **Figure 5**.

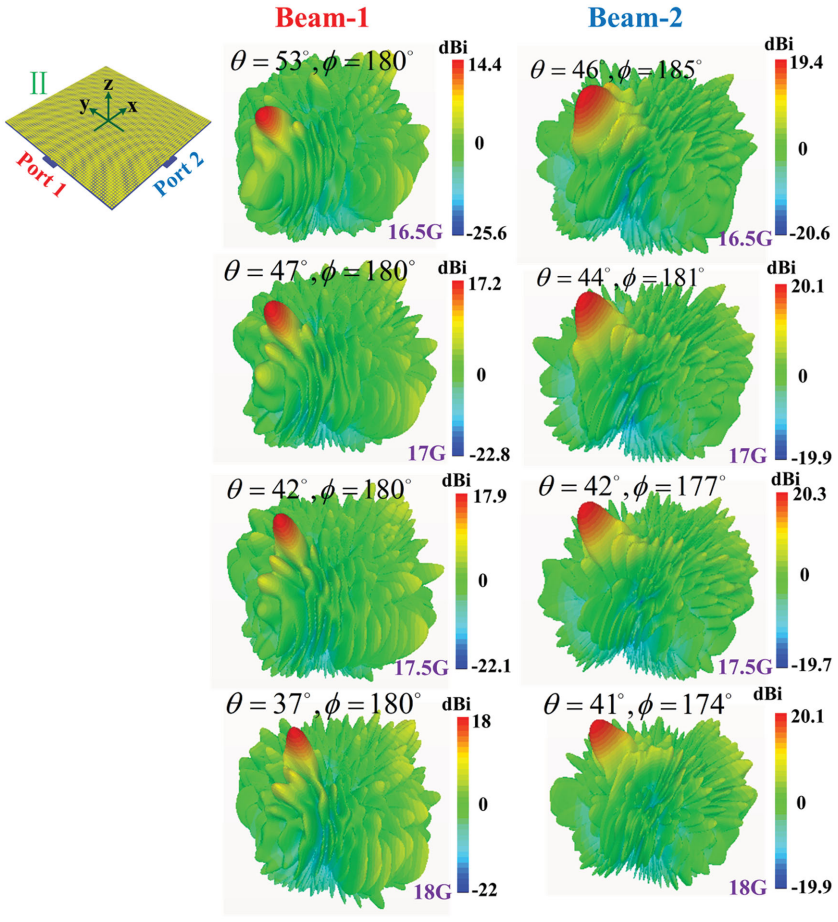

Figure 5. Full-wave simulated results of the holographic metasurface device (II). The two ports generate the single-beam under different polarizations with 1D and 2D frequency scanning from 16.5 to 18 GHz, respectively.

3. Fabrication and Experiment

To further validate the proposed method experimentally, we have fabricated the dual-functional holographic metasurface device (I) to control the double-beam radiations. The 1D scanning performance of Beams 1 and 2 can be easily verified by the far-field radiation patterns measured in our anechoic chamber, as shown in **Figure 6**a. The holographic metasurface device sample has the size of 192 × 192 mm^2, which is composed of 4096 impedance unit cells. In this sample, we choose F4B (the dielectric constant is 2.2) as the dielectric substrate and choose copper with tinning as the PEC. In measurements, we use the SMA connector as the monopole antenna to excite the holographic metasurface. When the platform carrying the metasurface rotates, the horn of the normal gain placed on the other side of the anechoic chamber can immediately record the

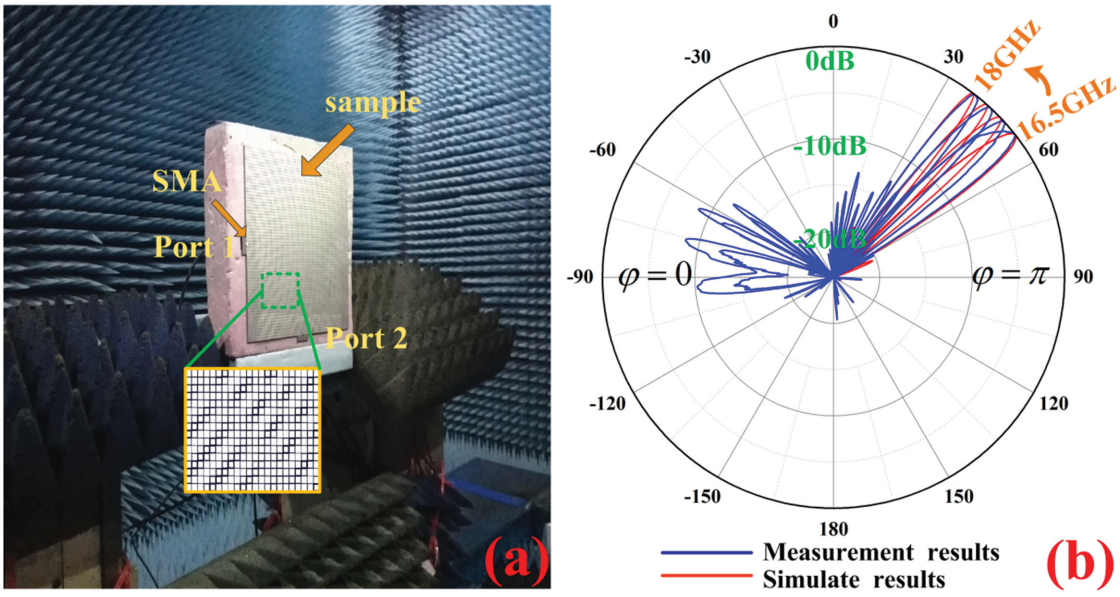

Figure 6. a) The fabricated sample of the holographic metasurface device (I) and the experimental setup. b) The measurement results of normalized far-field radiation patterns under the excitation of Port 1, showing excellent beam-scanning characteristics as the frequency changes from 16.5 to 18 GHz with the 0.5 GHz step. For the rotational symmetry of two excitation ports, the radiate beams generated by Port 2 have the same performance.

radiate intensity generated by the dual-functional device. Then, the 1D radiate pattern can be obtained using the experimental method. But it is hard to acquire the 2D (both of the azimuth and elevator directions) radiate pattern base on our measurement system. So we only measure the radiate performance of the device (I) which can only generate the 1D (the azimuth direction) scanning radiation under either exciting port. Figure 6a illustrates the experimental setup and Figure 6b gives the measured and simulated results at different frequencies from 16.5 to 18 GHz with the step of 0.5 GHz. We clearly observe that the experimental results have very good agreements with the numerical simulations. However, we note some side-lobes emerging in unimportant areas in the measurement results, which may be caused by the intrinsic noises in the anechoic chamber. If the metasurface has a larger size, we believe that the side lobes will be smaller.

4. Conclusions

We theoretically presented a new method of designing novel holographic metasurface devices which can accomplish arbitrarily dual-functional beam radiations. We integrated the double functions into a single isotropic impedance holographic metasurface which has no mutual interference. According to the proposed method, we designed two dual-functional devices that can realize double-beam radiations under the same polarization and single-beam radiations under the orthonormal polarizations, respectively. Based on our theoretical analysis, we found that the radiate beams can accomplish 1D or 2D spatial scanning controlled only by the frequency. Both full-wave simulations and experiment results showed excellent performance of the beam controls. The dual-functional frequency scanning devices have tremendous application potentials, such as in the new radar systems, foresight imaging systems, and calculating imaging systems. The proposed theory can be directly extended to deliver multifunctional holographic metasurface devices.

Acknowledgements

This work was supported by the National Science Foundation of China (Grant Nos. 61171024, 61171026, 61138001, 61302018, and 61401089), National High Tech (Grant No. 863) Projects (Grant Nos. 2011AA010202 and 2012AA030402), 111 Project (Grant No. 111-2-05), the Natural Science Foundation of the Jiangsu Province (Grant No. BK2012019), and the Scientific Research Foundation of Graduate School of Southeast University (Grant No. YBJJ1435).

Received: August 28, 2015
Revised: October 7, 2015
Published online: November 27, 2015

[1] D. R. Smith, J. B. Pendry, M. C. K. Wiltshire, *Science* **2004**, *305*, 788.
[2] D. Schurig, J. J. Mock, B. J. Justice, S. A. Cummer, J. B. Pendry, A. F. Starr, D. R. Smith, *Science* **2006**, *314*, 977.
[3] Y. Lai, H. Y. Chen, Z. Q. Zhang, C. T. Chan, *Phys. Rev. Lett.* **2009**, *102*, 093901.
[4] C. L. Holloway, M. A. Mohamed, E. F. Kuester, A. Dienstfrey, *IEEE Trans. Antennas Propag.* **2005**, *47*, 853.
[5] C. L. Holloway, E. F. Kuester, J. A. Gordon, J. O'Hara, J. Booth, D. R. Smith, *IEEE Trans. Antennas Propag.* **2012**, *54*, 10.
[6] R. E. Collin, *Field Theory of Guided Waves*, McGraw-Hill, New York **1960**.
[7] F. Falcone, T. Lopetegi, M. A. G. Laso, J. D. Baena, J. Bonache, M. Beruete, R. Marques, F. Martin, M. Sorolla, *Phys. Rev. Lett.* **2004**, *93*, 197401.
[8] N. Yu, P. Genevet, M. A. Kats, F. Aieta, J. P. Tetienne, F. Capasso, Z. Gaburro, *Science* **2011**, *334*, 333.
[9] C. Pfeiffer, A. Grbic, *Phys. Rev. Lett.* **2013**, *110*, 197401.

[10] S. Sun, Q. He, S. Xiao, Q. Xu, X. Li, L. Zhou, *Nat. Mater.* **2012**, *11*, 426.
[11] X. Ni, K. N. Emani, A. V. Kildishev, A. Boltasseva, V. M. Shalaev, *Science* **2012**, *35*, 427.
[12] M. Kang, T. H. Feng, H. T. Wang, J. Li, *Opt. Exp.* **2012**, *20*, 15882.
[13] R. Blanchard, G. Aoust, P. Genevet, N. Yu, M. A. Kats, Z. Gaburro, F. Capasso, *Phys. Rev. B* **2012**, *85*, 155457.
[14] B. Walther, C. Helgert, C. Rockstuhl, F. Setzpfandt, F. Eilenberger, E. B. Kley, F. Lederer, A. Tünnermann, T. Pertsch, *Adv. Mater.* **2012**, *24*, 6300.
[15] F. Monticone, N. M. Estakhri, A. Alu, *Phys. Rev. Lett.* **2013**, *110*, 203903.
[16] N. Yu, F. Capasso, *Nat. Mater.* **2014**, *13*, 139.
[17] L. Liu, X. Zhang, M. Kenney, X. Su, N. Xu, C. Ouyang, Y. Shi, J. Han, W. Zhang, S. Zhang, *Adv. Mater.* **2014**, *26*, 5031.
[18] M. Kim, A. M. H. Wong, G. V. Eleftheriades, *Phys. Rev. X* **2014**, *4*, 041042.
[19] S. Jiang, X. Xiong, Y. Hu, Y. Hu, G. Ma, R. Peng, C. Sun, M. Wang, *Phys. Rev. X* **2014**, *4*, 041042.
[20] X. Ni, A. V. Kildishev, V. M. Shalaev, *Nat. Commun.* **2013**, *4*, 2807.
[21] L. Huang, X. Chen, H. Mühlenbernd, H. Zhang, S. Chen, B. Bai, Q. Tan, G. Jin, K. Cheah, C. Qiu, J. Li, T. Zentgraf, S. Zhang, *Nat. Commun.* **2013**, *4*, 2808.
[22] G. Zheng, H. Mühlenbernd, M. Kenney, G. Li, T. Zentgraf, S. Zhang, *Nat. Nanotechol.* **2015**, *10*, 308.
[23] S. Larouche, Y. J. Tsai, T. Tyler, N. M. Jokerst, D. R. Smith, *Nat. Mater.* **2012**, *11*, 450.
[24] W. Kock, *Microwaves* **1968**, *7*, 46.
[25] W. H. Lee, *Appl. Opt.* **1970**, *9*, 639.
[26] G. Minatti, S. Maci, P. De Vita, A. Freni, M. Sabbadini, *IEEE Trans. Antennas Propag.* **2012**, *60*, 4998.
[27] A. M. Patel, A. Grbic, *IEEE Trans. Antennas Propag.* **2011**, *59*, 2087.
[28] Y. B. Li, X. Wan, B. G. Cai, Q. Cheng, T. J. Cui., *Sci. Rep.* **2014**, *4*, 6921.
[29] T. Zentgraf, J. Valentine, N. Tapia, J. Li, X. Zhang, *Adv. Mater.* **2010**, *22*, 2561.
[30] X. Wan, X. Shen, Y. Luo, T. J. Cui, *Laser Photonics Rev.* **2014**, *8*, 757.
[31] J. Lin, P. Genevet, M. A. Kats, N. Antoniou, F. Capasso, *Nano Lett.* **2013**, *13*, 4269.
[32] W. T. Chen, K. Yang, C. Wang, Y. Huang, G. Sun, I. Chiang, C. Y. Liao, W. Hsu, H. T. Lin, S. Sun, L. Zhou, A. Q. Liu, D. P. Tsai, *Nano Lett.* **2013**, *14*, 225.
[33] Y. Montelongo, J. Tenorio-Pearl, W. I. Milne, T. D. Wilkinson, *Nano Lett.* **2013**, *14*, 294.
[34] Y. B. Li, B. G. Cai, X. Wan, T. J. Cui, *Opt. Lett.* **2014**, *39*, 5888.
[35] Y. B. Li, B. G. Cai, Q. Cheng, T. J. Cui, *J. Phys. D: Appl. Phys.* **2015**, *48*, 035107.